6. P. V. Arriagada, J. H. Growdon, E. T. Hedley-Whyte, B. T. Hyman, *Neurology* **42**, 631 (1992).
7. C. Bancher, H. Braak, P. Fischer, K. A. Jellinger, *Neurosci. Lett.* **162**, 179 (1993).
8. A. L. Guillozet, S. Weintraub, D. C. Mash, M. M. Mesulam, *Arch. Neurol.* **60**, 729 (2003).
9. T. Gomez-Isla *et al.*, *Ann. Neurol.* **41**, 17 (1997).
10. J. Lewis *et al.*, *Science* **293**, 1487 (2001).
11. J. Gotz, F. Chen, J. van Dorpe, R. M. Nitsch, *Science* **293**, 1491 (2001).
12. S. Oddo, L. Billings, J. P. Kesslak, D. H. Cribbs, F. M. LaFerla, *Neuron* **43**, 321 (2004).
13. D. A. Bennett, J. A. Schneider, R. S. Wilson, J. L. Bienias, S. E. Arnold, *Arch. Neurol.* **61**, 378 (2004).
14. M. G. Spillantini, M. Goedert, *Trends Neurosci.* **21**, 428 (1998).
15. T. Ishihara *et al.*, *Neuron* **24**, 751 (1999).
16. J. Lewis *et al.*, *Nat. Genet.* **25**, 402 (2000).
17. J. Gotz, F. Chen, R. Barmettler, R. M. Nitsch, *J. Biol. Chem.* **276**, 529 (2001).
18. Y. Tatebayashi *et al.*, *Proc. Natl. Acad. Sci. U.S.A.* **99**, 13896 (2002).
19. C. Andorfer *et al.*, *J. Neurochem.* **86**, 582 (2003).
20. M. Hutton *et al.*, *Nature* **393**, 702 (1998).
21. M. Gossen, H. Bujard, *Proc. Natl. Acad. Sci. U.S.A.* **89**, 5547 (1992).
22. M. Mayford *et al.*, *Science* **274**, 1678 (1996).
23. M. A. Westerman *et al.*, *J. Neurosci.* **22**, 1858 (2002).
24. G. Chen *et al.*, *Nature* **408**, 975 (2000).
25. J. Lewis, M. Hutton, unpublished observations.
26. M. Arrasate, S. Mitra, E. S. Schweitzer, M. R. Segal, S. Finkbeiner, *Nature* **431**, 805 (2004).
27. We thank A. Michael for support; S. Iyadurai and G. Carlson for critical discussions; N. Nash, M. Sherman, A. Hanna, J. Knight, C. Zehr, S. Nelson, and D. Norton for technical help; and P. Sharpe for secretarial assistance. Supported by grants from the NIH (P01-AG15453, R01-026252 to K.H.A.; R01-AG26249, R01-AG08487 to B.H; T31-AG00277 to T.S.; R01-NS46355 to J.L.).

Supporting Online Material
www.sciencemag.org/cgi/content/full/309/5733/476/DC1
Materials and Methods
Figs. S1 to S8
References and Notes

18 April 2005; accepted 27 May 2005
10.1126/science.1113694

Mitochondrial DNA Mutations, Oxidative Stress, and Apoptosis in Mammalian Aging

G. C. Kujoth,[1] A. Hiona,[2] T. D. Pugh,[3] S. Someya,[4] K. Panzer,[1] S. E. Wohlgemuth,[2] T. Hofer,[2] A. Y. Seo,[2] R. Sullivan,[5] W. A. Jobling,[6] J. D. Morrow,[7] H. Van Remmen,[8] J. M. Sedivy,[6] T. Yamasoba,[9] M. Tanokura,[4] R. Weindruch,[3] C. Leeuwenburgh,[2] T. A. Prolla[1]*

Mutations in mitochondrial DNA (mtDNA) accumulate in tissues of mammalian species and have been hypothesized to contribute to aging. We show that mice expressing a proofreading-deficient version of the mitochondrial DNA polymerase γ (POLG) accumulate mtDNA mutations and display features of accelerated aging. Accumulation of mtDNA mutations was not associated with increased markers of oxidative stress or a defect in cellular proliferation, but was correlated with the induction of apoptotic markers, particularly in tissues characterized by rapid cellular turnover. The levels of apoptotic markers were also found to increase during aging in normal mice. Thus, accumulation of mtDNA mutations that promote apoptosis may be a central mechanism driving mammalian aging.

Mitochondria are the main source of cellular adenosine triphosphate and play a central role in a variety of cellular processes. These include fatty acid β-oxidation, phospholipid biosynthesis, calcium signaling, reactive oxygen species (ROS) generation, and apoptosis. Because the mitochondrion contains its own ~16-kilobase circular DNA, a central role for mtDNA mutations in aging has been postulated (*1*, *2*). Indeed, mtDNA mutations have been shown to accumulate with aging in several tissues of various species (*3*–*7*). The causal role of mtDNA mutations in mammalian aging is supported by a recent study demonstrating that mice with a mitochondrial mutator phenotype develop several aging phenotypes (*8*). Here, we used similar mice to investigate the cellular mechanisms by which mtDNA mutations contribute to aging.

We cloned the mouse POLG locus, *PolgA*, and used gene targeting in embryonic stem cells to introduce an AC → CT two-base substitution that corresponds to positions 1054 and 1055 of the *PolgA* cDNA (fig. S1) (*9*). This mutation results in a critical residue substitution in the conserved exonuclease domain of POLG, impairing its proofreading ability (*8*). Germline transmission of the mutation produced $PolgA^{D257A/+}$ mice, which were intercrossed to generate homozygous $PolgA^{D257A/D257A}$ mice, hereafter denoted D257A. Young D257A mice were indistinguishable from wild-type littermates, but long-term follow-up revealed a striking premature aging phenotype beginning at ~9 months of age, consisting of hair loss, graying, and kyphosis (Fig. 1, A and B). The mutant mice had a reduced life span (for

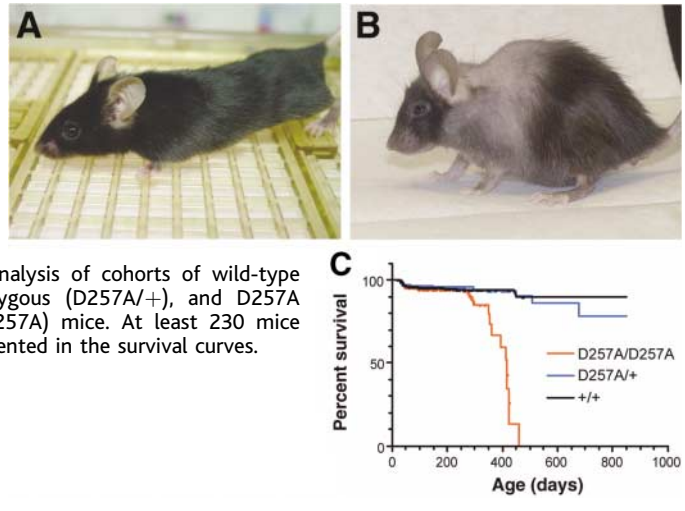

Fig. 1. D257A mice display a premature aging phenotype. Shown are wild-type (**A**) and D257A mice (**B**) at ~13 months of age. Progeroid features, including hair loss, graying, and kyphosis, become apparent at ~9 months of age. (**C**) Kaplan-Meier survival analysis of cohorts of wild-type (+/+), D257A heterozygous (D257A/+), and D257A homozygous (D257A/D257A) mice. At least 230 mice per genotype are represented in the survival curves.

[1]Departments of Genetics and Medical Genetics, University of Wisconsin, Madison, WI 53706, USA. [2]Department of Aging and Geriatric Research, College of Medicine, Institute on Aging, Biochemistry of Aging Laboratory, University of Florida, Gainesville, FL 32610-0107, USA. [3]Department of Medicine and Veterans Administration Hospital, University of Wisconsin, Madison, WI 53705-2286, USA. [4]Department of Applied Biological Chemistry, University of Tokyo, Bunkyo-ku, Tokyo 113-8657, Japan. [5]Waisman Center, University of Wisconsin, Madison, WI 53705-2280, USA. [6]Department of Molecular Biology, Cell Biology and Biochemistry and Center for Genomics and Proteomics, Brown University, Providence, RI 02912, USA. [7]Departments of Medicine and Pharmacology, Vanderbilt University School of Medicine, Nashville, TN 37232, USA. [8]Department of Cellular and Structural Biology and Barshop Institute on Longevity and Aging Studies, University of Texas Health Center at San Antonio, San Antonio, TX 78284, USA. [9]Department of Otolaryngology, University of Tokyo, Bunkyo-ku, Tokyo 113-8657, Japan.

*To whom correspondence should be addressed. E-mail: taprolla@wisc.edu

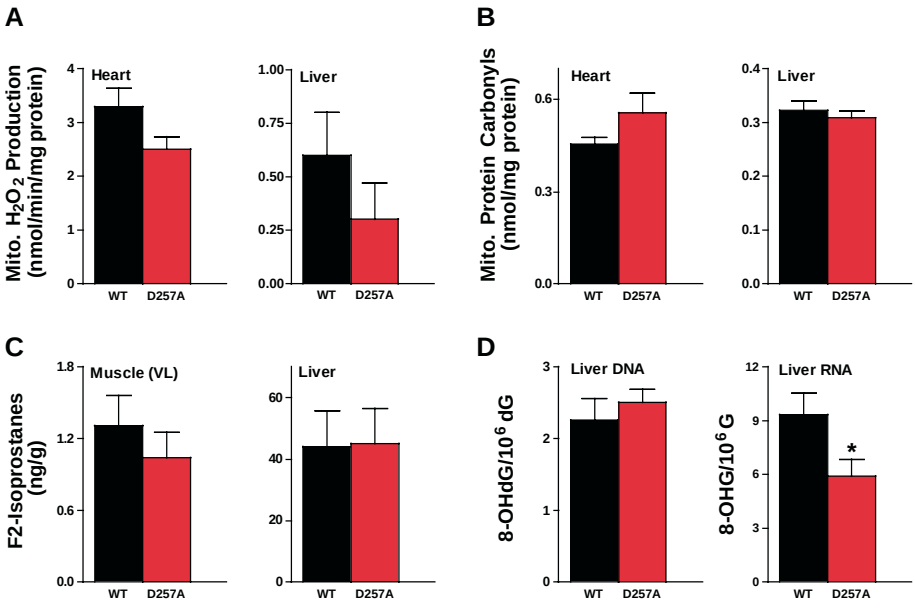

Fig. 2. Oxidative stress markers in isolated mitochondria and tissues from D257A mice. (**A**) Hydrogen peroxide production was measured by a sensitive fluorometric assay in mitochondria from wild-type (WT) and D257A mice at 9 months of age ($N \geq 8$). (**B**) Protein carbonyl levels, a marker of protein oxidation, were measured by an enzyme immunoassay in isolated mitochondria from WT and D257A mice at 9 months of age ($N \geq 7$). (**C**) F2-isoprostanes were measured by gas chromatography–negative ion chemical ionization mass spectrometry in liver and skeletal muscle (vastus lateralis) tissues from 6-month-old WT and D257A mice ($N = 6$). (**D**) Oxidative damage to DNA (8-OHdG) and RNA (8-OHG) was measured by high-performance liquid chromatography in liver tissue of 9-month-old WT and D257A mice ($N = 9$). *$P < 0.05$; error bars represent SEM.

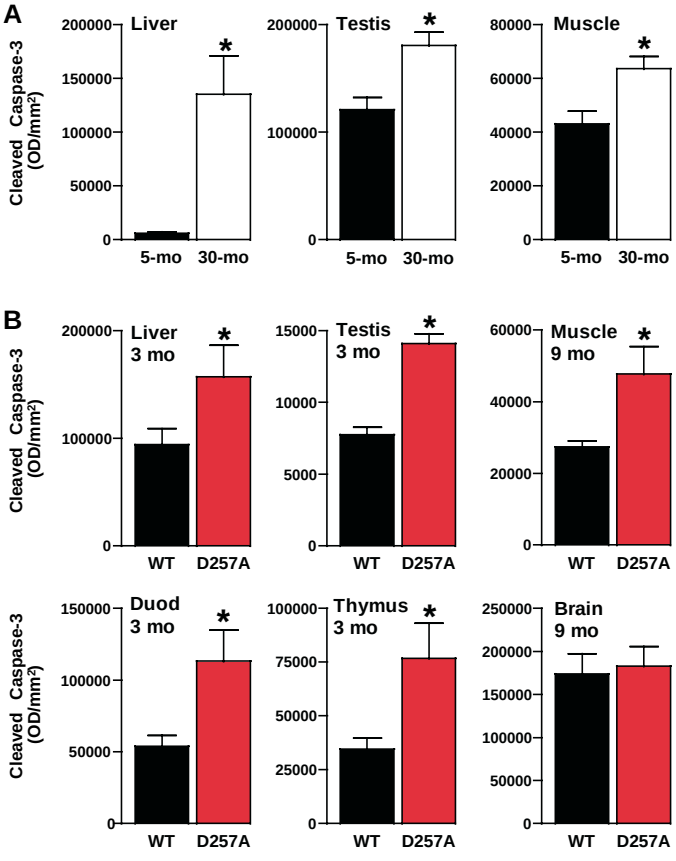

Fig. 3. Caspase activation in D257A mice and in normal aging. (**A**) Comparison of young (5 month) versus old (30 month) wild-type tissues. (**B**) Comparison of wild-type (WT) and D257A tissues at 3 months and 9 months of age. Activation of caspase-3 requires proteolytic processing of its inactive zymogen into activated fragments. The antibody used detects endogenous levels of the large fragment (17 to 19 kD) of activated caspase-3 resulting from cleavage adjacent to Asp^{175}. Extracts of tissues from WT and D257A mice of the indicated ages were subjected to SDS–polyacrylamide gel electrophoresis (PAGE) and probed with a rabbit monoclonal antibody to cleaved caspase-3 (5A1, Cell Signaling, Beverly, MA). Units are arbitrary OD units. For all tissues shown except brain, the difference between WT and D257A mice was significant ($N = 6$ to 8, *$P < 0.05$); error bars represent SEM. Duod, duodenum; Muscle, gastrocnemius.

D257A mice, maximum survival 460 days, median survival 416 days; for wild-type littermates, maximum and median survival >850 days; $P < 0.0001$; Fig. 1C) and displayed several overt phenotypes in tissues undergoing rapid cellular turnover. These phenotypes were age-related and included thymic involution, testicular atrophy associated with the depletion of spermatogonia, loss of bone mass, loss of intestinal crypts, progressive decrease in circulating red blood cells, and weight loss (figs. S2 to S4).

Age-related hearing loss (presbycusis) is a hallmark of aging in multiple species, including mice (*10*) and humans (*11*), and has been correlated with the age-related accumulation of mtDNA mutations in auditory tissue. Hearing loss can be monitored by an elevation in auditory-evoked brainstem response (ABR). We conducted ABR analysis and observed no difference in auditory function between wild-type and D257A mice at 2 months of age (fig. S5G), but we found marked elevation of ABR thresholds at 4, 8, and 16 kHz ($P < 0.0001$) in D257A mice by 9 months of age, indicating severe hearing loss (fig. S5H). Histological analysis revealed age-related loss of spiral ganglion neurons (fig. S5), a feature of presbycusis (*12*). Thus, accumulation of mtDNA mutations can have a causal role in presbycusis.

Aging in rodents (*13*) and humans (*14*) is also characterized by loss of muscle mass (sarcopenia). Consistent with a causal role for mtDNA mutations in sarcopenia, the D257A mice displayed age-related loss of skeletal muscle. At 3 months of age, muscle weight in the D257A mice was similar to that of wild-type mice (fig. S6A); at 9 months of age, however, the mutant mice showed a significant reduction in the weight of both gastrocnemius ($P < 0.002$, ~10% decrease) and quadriceps ($P < 0.005$, ~10% decrease) muscles (fig. S6B). Therefore, age-related accumulation of mtDNA mutations is likely to contribute to sarcopenia.

To determine whether mtDNA mutations accumulated to varying extents in different tissues of the D257A mice, we sequenced a 525–base pair (bp) region of mtDNA that spans the control region, as well as a 487-bp region of the *COX1* gene. Sequencing revealed that the frequency of mtDNA mutations in the mutant mice was ~3 to 8 times that in wild-type mice for most tissues examined (fig. S7). Surprisingly, the frequency of mtDNA mutations in 5-month-old wild-type mice was as high as 2.1×10^{-4} in the *COX1* gene and 5.9×10^{-4} in the control region. This corresponds to average mutation frequencies of ~4 and ~10 mutations per mitochondrial genome, respectively.

A fraction of the oxygen consumed by cells results in the production of superoxide ($O_2^{\bullet-}$) in mitochondria, which is dismutated to hydrogen peroxide (H_2O_2) by superoxide dismutase. The main tenet of the free radical theory

of aging (*15*) is that aging is due to the progressive accrual of ROS-inflicted damage, including mtDNA mutations, the accumulation of which has been postulated to lead to a "vicious cycle" of further mitochondrial ROS generation and mitochondrial dysfunction (*1*, *2*). To test this hypothesis, we measured H_2O_2 produced by mitochondria isolated from the heart and liver of young and old (3 months versus 9 months) D257A and wild-type mice. Levels of H_2O_2 were not significantly different between genotypes in either young or old heart or liver mitochondria (Fig. 2A) (fig. S8A). We also assayed protein carbonyls, a marker of oxidative damage to proteins, and found no significant differences between 9-month-old D257A and wild-type mice in mitochondrial (Fig. 2B) or cytosolic fractions (fig. S8B) of either heart or liver. Thus, despite increased mutational load, mitochondria from D257A mice do not show increased oxidative stress.

We next examined additional markers of ROS-induced damage in tissues of D257A and wild-type mice. We measured F2-isoprostanes, a marker of lipid peroxidation (*16*), in liver, skeletal muscle (Fig. 2C), and heart (fig. S8C), and observed no significant differences between 6-month-old D257A mice and wild-type controls. We also examined oxidative damage to RNA and DNA in 9-month-old D257A and wild-type mice. Liver DNA from wild-type and mutant mice had similar levels of 8-hydroxy-2′-deoxyguanosine (8-OHdG) (Fig. 2D). Interestingly, liver RNA from the D257A mice had lower steady-state levels of 8-hydroxyguanosine (8-OHG) relative to samples from wild-type mice (Fig. 2D, $P < 0.05$). Thus, our observations do not support the idea that mtDNA mutations contribute to increased ROS production and oxidative stress in mitochondria with age.

One possible mechanism for the phenotypes in mitotic tissues of D257A mice is a defect in cellular proliferation. We derived mouse embryonic fibroblast lines (MEFs) from D257A and wild-type littermates and measured the number of cell doublings before senescence. At 20% oxygen, both wild-type and D257A MEFs underwent rapid replicative senescence, whereas neither underwent senescence or reduced growth after 40 days of culture at 2% oxygen (fig. S9). Thus, accelerated aging in D257A mice is not likely to be due to an intrinsic defect in cellular proliferation, or to accelerated cellular senescence.

In the mitochondrial pathway of apoptosis, mitochondrial dysfunction can lead to mitochondrial outer membrane permeabilization, the release of cytochrome c into the cytosol, and the activation of a key effector protease, caspase-3, by proteolytic cleavage (*17*, *18*). To determine whether an increased level of cleaved caspase-3 is a feature of normal aging, we examined tissues of 5-month-old and 30-month-old wild-type mice by immunoblotting. Cleaved caspase-3 levels increased with aging in liver, skeletal muscle, testis (Fig. 3A), and heart (fig. S10A) of wild-type mice by ~50% or greater. We also monitored the extent of apoptosis in tissues of D257A and wild-type mice. Levels of cleaved caspase-3 were significantly elevated in the cytosolic fractions of duodenum, liver, testis, and thymus of 3-month-old D257A mice relative to wild-type controls (Fig. 3B), and this induction preceded phenotypes in most tissues. Levels of cleaved caspase-3 were not altered in 3-month-old D257A skeletal muscle and brain relative to wild-type samples (fig. S10B), which suggests that postmitotic tissues may be more resistant to the induction of apoptosis mediated by mtDNA mutations. Cleaved caspase-3 levels were increased, however, in D257A skeletal muscle at 9 months of age relative to controls (Fig. 3B), a time at which mutant animals displayed loss of muscle mass. Thus, normal aging is associated with the activation of a caspase-3–mediated apoptotic pathway in several tissues, and D257A mice display an early onset of this phenotype.

Apoptosis is also associated with nuclear DNA fragmentation. Because the intestinal epithelium, thymus, and testis were severely affected in D257A mice, we examined these tissues with the TUNEL (terminal deoxynucleotidyl transferase–mediated deoxyuridine triphosphate nick end labeling) assay, which detects apoptotic cells in situ. The 3-month-old D257A mice showed significantly more TUNEL positive cells relative to wild-type mice in all tissues examined (Fig. 4). Together, these findings strongly suggest that loss of critical, irreplaceable cells through apoptosis is a central mechanism of tissue dysfunction associated with the accumulation of mtDNA mutations.

We have demonstrated that accelerated development of aging phenotypes through mtDNA mutations can occur in the absence of increased ROS production or oxidative stress, and that tissue dysfunction is likely to arise through increased apoptosis. Moreover, we have shown that increased caspase-3 activation occurs in multiple tissues with normal aging. Tissues that are composed of mitotic cells display early caspase-3 activation in D257A mice, whereas skeletal muscle displays a later increase in cleaved caspase-3 and associated tissue degeneration. It is also clear that some cell types, such as spiral ganglion neurons, are exquisitely sensitive to the effects of age-related accumulation of mtDNA mutations. Because D257A mice display high levels of mtDNA mutations, it is possible that some of the phenotypes in these animals may be due to

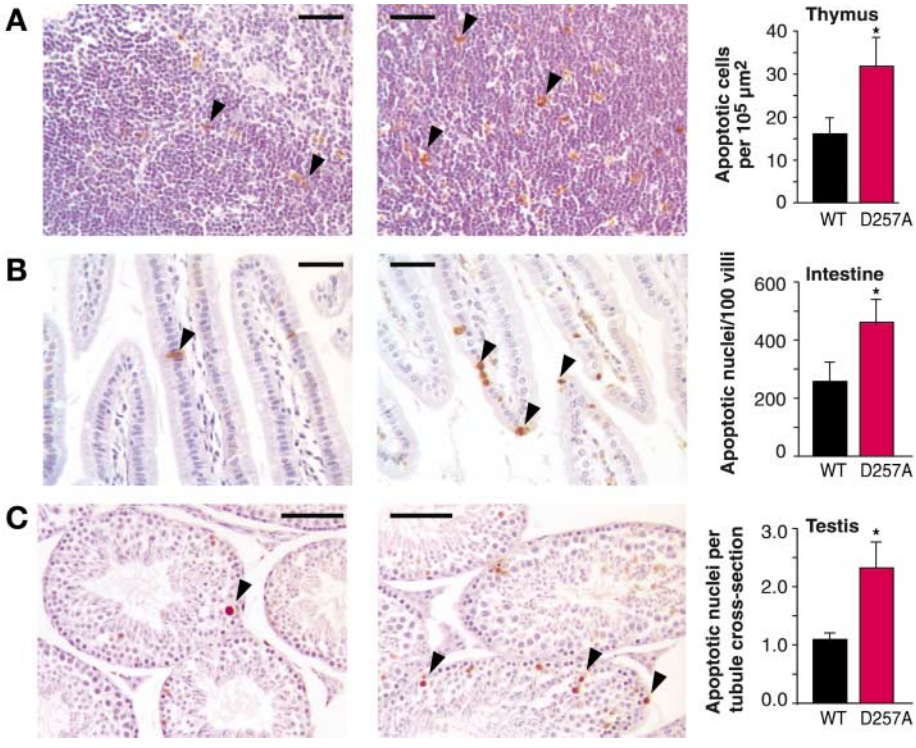

Fig. 4. Quantification of apoptosis by TUNEL in thymus (**A**), small intestine (**B**), and testis (**C**) of 3-month-old WT (left panels) and D257A (center panels) mice. Arrowheads indicate TUNEL-positive apoptotic nuclei. Numbers of apoptotic nuclei per 10^5 µm² section (thymus), per 100 villi (intestine), and per seminiferous tubule cross section (testis) were counted in hematoxylin-counterstained sections from the indicated genotypes. Each bar represents apoptotic nuclei from intestinal, thymus, and testis sections of at least four mice per genotype. *$P < 0.05$; error bars represent SEM. Scale bar, 100 µm.

complete exhaustion of tissue regenerative capacity, a process that may not be as severe in normal aging. However, the wide tissue distribution of phenotypes in D257A mice suggests that the age-related accumulation of mtDNA mutations reported in several species (*3*–*7*) contributes to physiological decline.

The concept that DNA damage contributes to aging is supported by the finding that humans and mice carrying mutations in several genes involved in DNA repair, including *Ercc2* (*Xpd*) (*19*), *Xrcc5* (*Ku86*) (*20*), and *Wrn* (*21*), display premature aging syndromes. It is likely that several types of DNA damage contribute to the aging process, and our findings suggest that apoptosis and subsequent loss of irreplaceable cells may be an important mechanism of aging in mammals. In agreement with this hypothesis, caloric restriction, the only nutritional intervention that retards aging, delays the accumulation of mtDNA mutations (*22*) and reduces mitochondria-mediated apoptotic pathways (*23*, *24*).

References and Notes

1. D. Harman, *J. Am. Geriatr. Soc.* **20**, 145 (1972).
2. J. E. Fleming, J. Miquel, S. F. Cottrell, L. S. Yengoyan, A. C. Economos, *Gerontology* **28**, 44 (1982).
3. Y. Wang *et al.*, *Proc. Natl. Acad. Sci. U.S.A.* **98**, 4022 (2001).
4. S. Melov, D. Hinerfeld, L. Esposito, D. C. Wallace, *Nucleic Acids Res.* **25**, 974 (1997).
5. M. Corral-Debrinski *et al.*, *Nat. Genet.* **2**, 324 (1992).
6. C. M. Lee, S. S. Chung, J. M. Kaczkowski, R. Weindruch, J. M. Aiken, *J. Gerontol.* **48**, B201 (1993).
7. M. Khaidakov, R. H. Heflich, M. G. Manjanatha, M. B. Myers, A. Aidoo, *Mutat. Res.* **526**, 1 (2003).
8. A. Trifunovic *et al.*, *Nature* **429**, 417 (2004).
9. See supporting data on *Science* Online.
10. Q. Y. Zheng, K. R. Johnson, L. C. Erway, *Hear. Res.* **130**, 94 (1999).
11. M. A. Gratton, A. E. Vazquez, *Curr. Opin. Otolaryngol. Head Neck Surg.* **11**, 367 (2003).
12. E. M. Keithley, C. Canto, Q. Y. Zheng, N. Fischel-Ghodsian, K. R. Johnson, *Hear. Res.* **188**, 21 (2004).
13. J. Wanagat, Z. Cao, P. Pathare, J. M. Aiken, *FASEB J.* **15**, 322 (2001).
14. J. Lexell, C. C. Taylor, M. Sjostrom, *J. Neurol. Sci.* **84**, 275 (1988).
15. D. Harman, *J. Gerontol.* **11**, 298 (1956).
16. L. J. Roberts 2nd, J. D. Morrow, *Cell. Mol. Life Sci.* **59**, 808 (2002).
17. D. R. Green, G. Kroemer, *Science* **305**, 626 (2004).
18. M. O. Hengartner, *Nature* **407**, 770 (2000).
19. J. de Boer *et al.*, *Science* **296**, 1276 (2002).
20. H. Vogel, D. S. Lim, G. Karsenty, M. Finegold, P. Hasty, *Proc. Natl. Acad. Sci. U.S.A.* **96**, 10770 (1999).
21. S. Chang *et al.*, *Nat. Genet.* **36**, 877 (2004).
22. L. E. Aspnes *et al.*, *FASEB J.* **11**, 573 (1997).
23. R. R. Shelke, C. Leeuwenburgh, *FASEB J.* **17**, 494 (2003).
24. H. Y. Cohen *et al.*, *Science* **305**, 390 (2004).

25. We thank J. Warren for stem cell injections, S. Kinoshita for histological processing, and D. Carlson for support in mouse colony management. Supported by NIH grants AG021905 (T.A.P.), AG18922 (R.W.), AG17994 (C.L.), AG21042 (C.L.), DK48831, GM15431, and RR00095 (J.D.M.), and AG16694 (J.M.S.); by NIH training grants T32 AG00213 (G.C.K.) and T32 GM07601 (W.A.J.); and by American Heart Association predoctoral fellowship 0415166B (A.H.). R.W. and T.A.P. are founders and members of the board of LifeGen Technologies, a company focused on nutritional genomics, including the impact of nutrients and caloric restriction on the aging process.

Supporting Online Material

www.sciencemag.org/cgi/content/full/309/5733/481/DC1
Materials and Methods
Figs. S1 to S10

11 March 2005; accepted 25 May 2005
10.1126/science.1112125

Chromatic Adaptation of Photosynthetic Membranes

Simon Scheuring[1]* and James N. Sturgis[2]

Many biological membranes adapt in response to environmental conditions. We investigated how the composition and architecture of photosynthetic membranes of a bacterium change in response to light, using atomic force microscopy. Despite large modifications in the membrane composition, the local environment of core complexes remained unaltered, whereas specialized paracrystalline light-harvesting antenna domains grew under low-light conditions. Thus, the protein mixture in the membrane shows eutectic behavior and can be mimicked by a simple model. Such structural adaptation ensures efficient photon capture under low-light conditions and prevents photodamage under high-light conditions.

The atomic force microscope (*1*) is a powerful tool for imaging membrane proteins (*2*). Recently, the first images at submolecular resolution of native membranes have shed light on the architecture of the photosynthetic apparatus in different photosynthetic bacteria, i.e., *Blastochloris* (*Blc.*) *viridis* (*3*), *Rhodospirillum* (*Rsp.*) *photometricum* (*4*, *5*), *Rhodobacter* (*Rb.*) *sphaeroides* (*6*), and *Rb. blasticus* (*7*). For photosynthesis to remain efficient, the composition of the photosynthetic apparatus alters under different light conditions. In many purple photosynthetic bacteria, this chromatic adaptation involves modulation of the quantity of peripheral and core light-harvesting (LH) complexes and, in some species, involves the expression of LH complexes with modified absorption (*8*).

How is the architecture of the photosynthetic membrane modulated during adaptation to different environmental conditions? Here we present a comparative study of native membranes from high- and low-light–adapted *Rsp. photometricum* cells. We used high-resolution atomic force microscopy (AFM) to investigate the structure, molecular interactions, and assembly of the membrane complexes. We imaged the cytoplasmic membrane surface of intact chromatophores (fig. S1), resorting neither to nanodissection (*4*) nor detergent treatment (*6*). The membrane components segregated into two distinct regions: (i) amorphous domains containing reaction centers (RCs) with defined molar ratios of LH1 and LH2, and (ii) paracrystalline peripheral antenna (LH2) domains. This two-phase structure could have an important functional role, as the antenna fields may exclude quinone/quinol (Q/QH_2). This will markedly reduce the membrane volume accessible to quinones and so accelerate transfer along preferential routes. As quinone diffusion is much slower than light capture, energy transfer, and the other electron transfer reactions (*9*), this effect will increase efficiency. Our analysis further suggests a model for understanding the interactions between the different components.

Qualitatively, we found the same photosynthetic complexes in high-light– and low-light–adapted membranes. Comparison with previous structural data for LH2 (*5*, *10*–*15*), LH1-RC core complexes (*3*, *7*, *16*–*18*), and RCs (*19*, *20*) allowed us to identify the small rings (~50 Å in diameter) as LH2 and the large elliptical complexes as core complexes. The LH1 assembly of the core complex forms a closed ellipse of 16 LH1 subunits surrounding an elongated RC (Fig. 1, A and B). The *Rsp. photometricum* core complex is reminiscent of that observed in *Blc. viridis* (*3*) and *Rsp. rubrum* (*16*), monomeric and without a gap in the LH1, unlike either the monomeric, W-containing core complex of *Rps. palustris* (*18*) or the PufX-containing dimeric complexes of *Rb. sphaeroides* (*21*–*23*) and *Rb. blasticus* (*7*). The functional consequences of the structural variability of core complexes remain unclear (*24*). The LH2 complexes were nonameric rings (Fig. 1D). Rarely, LH2 that either lack or have extra subunits are found (*5*). Such LH complexes with extra subunits (Fig. 1C) were found in both types of membranes and could consist of LH1 or LH2 subunits or mixtures

[1]Institut Curie, Unité Mixte de Recherche–CNRS 168, 11 rue Pierre et Marie Curie, 75231 Paris Cedex 05, France. [2]Unité Propre de Recherche–9027 Laboratoire d'Indenierie de Systemes Macromoleculaires, Institut de Biologie Structurale et Microbiologie, CNRS, 31 Chemin Joseph Aiguier, 13402 Marseille Cedex 20, France.

*To whom correspondence should be addressed. E-mail: simon.scheuring@curie.fr

Mitochondrial DNA Mutations, Oxidative Stress, and Apoptosis in Mammalian Aging

G. C. Kujoth, A. Hiona, T. D. Pugh, S. Someya, K. Panzer, S. E. Wohlgemuth, T. Hofer, A. Y. Seo, R. Sullivan, W. A. Jobling, J. D. Morrow, H. Van Remmen, J. M. Sedivy, T. Yamasoba, M. Tanokura, R. Weindruch, C. Leeuwenburgh and T. A. Prolla

Science **309** (5733), 481-484.
DOI: 10.1126/science.1112125